Role of Nitrogen Defects in Graphitic Carbon Nitride for Visible-Light-Driven Hydrogen Evolution

*Jiawei Xue, Mamoru Fujitsuka, and Tetsuro Majima**

The Institute of Scientific and Industrial Research (SANKEN), Osaka University, Mihogaoka 8-1, Ibaraki, Osaka 567-0047, Japan

Section 1. Experimental Details

1.1. Synthesis Method

N-deficient g-C_3N_4 (DCN) was synthesized via a KOH-assisted thermal polymerization method.[1] Briefly, 15 g of urea was dissolved with stirring into the KOH solution (1.0 g KOH in 30 mL of H_2O), and then the as-obtained solution evaporated to dryness in an oven at 80 °C overnight. The solid mixtures of urea and KOH were then calcined at 550 °C in a muffle furnace for 4 h using a heating rate of 2 °C min^{-1}. For comparison, bulk g-C_3N_4 (CN) was also synthesized parallelly in the absence of KOH.

1.2. Characterization

The samples were characterized using X-ray diffraction (XRD, Rigaku, Smartlab; operated at 40 kV and 200 mA, Cu Kα source), scanning electron microscopy (SEM, JEOL, JSM-6330FT). The XPS measurements were carried out on a PHI X-tool 8ULVAC-PHI instrument. Fourier transformed infrared (FTIR) measurements were conducted by a PerkinElmer spectrometer. The steady-state diffuse reflection spectra were measured on a UV-vis-NIR spectrophotometer (Jasco, V-570) at room temperature. Electro paramagnetic resonance (EPR) spectra were recorded on a JEOL JES-RE2X electron spin resonance spectrometer at room temperature.

1.3. Photocatalytic Activity Tests

3 mg of the sample was dispersed in 5 mL triethanolamine (TEOA)-H_2O solution

(V_{TEOA}:V_{H2O} = 1:4) and added into a 35 mL cylinder reactor. Then, 3 wt% (respect to Pt, acting as co-catalysts) $H_2PtCl_6 \cdot 6H_2O$ was deposited onto the photocatalyst by the photodeposition method. The reactor was sealed, and then bubbled with argon through the reactor for 30 min to completely remove the dissolved oxygen and ensure the reactor was in an anaerobic condition. Subsequently, the suspension with continuous stirring was irradiated under a UV-LED source (POT-365; 100 mW cm^{-2}) or a Xe lamp (Asahi Spectra, HAL-320; 350 mW cm^{-2}) equipped with a 420 nm or 460 nm cutoff filter at room temperature. H_2 production was measured by using Shimadzu GC-8A gas chromatograph equipped with an MS-5A column and a thermal conductivity detector. The apparent quantum efficiency (AQE) for H_2 production at different wavelengths (420, 460, 500, 560 nm) of the monochromatic light was calculated via the following equation: AQE = (2 × number of H_2 molecules/number of incident photons) × 100 %.

1.4. Transient Absorption Measurements

The femtosecond time-resolved transient absorption (TA) spectra were measured by the pump and probe method using a regeneratively amplified titanium sapphire laser (Spectra-Physics, Spitfire Pro F, 1 kHz) pumped by a Nd:YLF laser (Spectra-Physics, Empower 15). The seed pulse was generated by a titanium sapphire laser (Spectra-Physics, Mai Tai VFSJW; FWHM 80 fs). The output (420 nm or 560 nm, 4 μJ per pulse) of the optical parametric amplifier (Spectra-Physics, OPA-800CF-1) was used as the excitation pulse. A white light continuum pulse, which was generated by focusing the residual of the fundamental light on a sapphire crystal after the computer controlled optical delay, was divided into two parts and used as the probe and the reference lights, of which the latter was used to compensate for the laser fluctuation. Both probe and reference lights were directed to the sample powder coated on the glass substrate, and the reflected lights were detected by a linear InGaAs array detector equipped with the polychromator (Solar, MS3504). The pump pulse was chopped with a mechanical chopper synchronized to one-half of the laser repetition rate, resulting in a pair of spectra with and without the pump, from which the absorption change (% Abs) induced by the pump pulse was estimated. All measurements were carried out at room temperature.

1.5. Density Functional Theory (DFT) Calculations

All calculations were carried out using CASTEP, as implemented in Materials Studio 8.0. Nonlocal exchange and correlation energies were treated with the Perdew-Burke-Ernzerhof (PBE) functional, which was based on the generalized gradient approximation (GGA). a 500 eV cutoff was assigned to the plane-wave basis set and the Brillouin zone was sampled by 3×3×4 k-points. In the geometry optimization process, the energy convergence tolerance and maximum force were set to be 5×10^{-6} eV per atom and 0.01 eV $Å^{-1}$, respectively.

Section 2. Supplementary Data

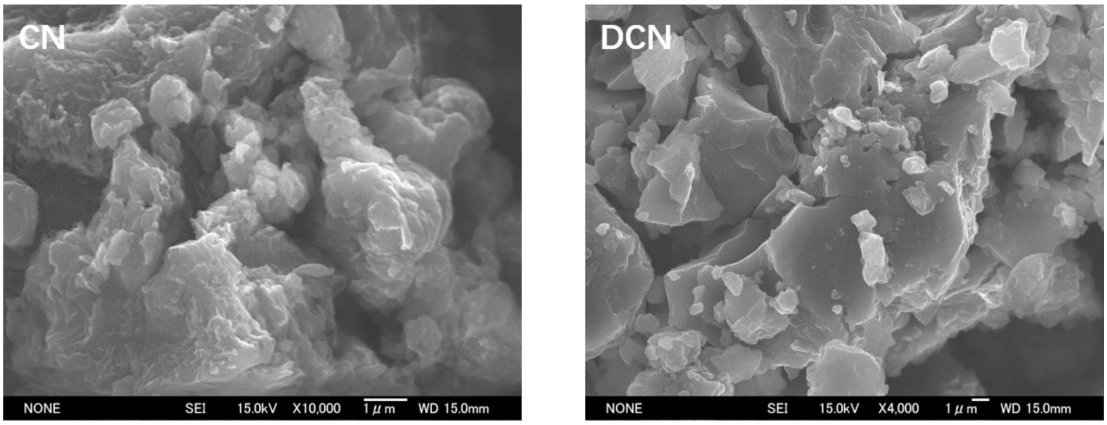

Figure S1. SEM images of CN and DCN.

Table S1. N/C atomic ratios of CN and DCN determined by the elemental analysis (EA) and XPS.

Samples	**EA**				**XPS**				
	N (wt%)	C (wt%)	H (wt%)	N/C (atomic)	N (at%)	C (at%)	O (at%)	K (at%)	N/C (atomic)
CN	57.54	32.66	1.95	1.51	54.49	42.94	2.56	-	1.27
DCN	56.18	33.73	2.08	1.43	46.81	43.74	5.67	3.78	1.07

It should be mentioned here that the N/C atomic ratio in CN obtained by EA is generally higher than the stoichiometric ratio of 1.33 due to the residual amino groups originating from incomplete condensation of the precursor.[2] In contrast, the N/C atomic ratio in CN obtained by XPS is lower than the stoichiometric one because the thermal oxidation etching would remove the surface N atoms.[3]

Because EA provides the information of the whole sample, while XPS can only provide surface information, the percentage of N vacancies is calculated to be 5.3 % in DCN according to EA results. However, we cannot determine the percentage of cyano groups in DCN based on EA results because the formation of cyano groups does not result in N loss in the bulk.[1]

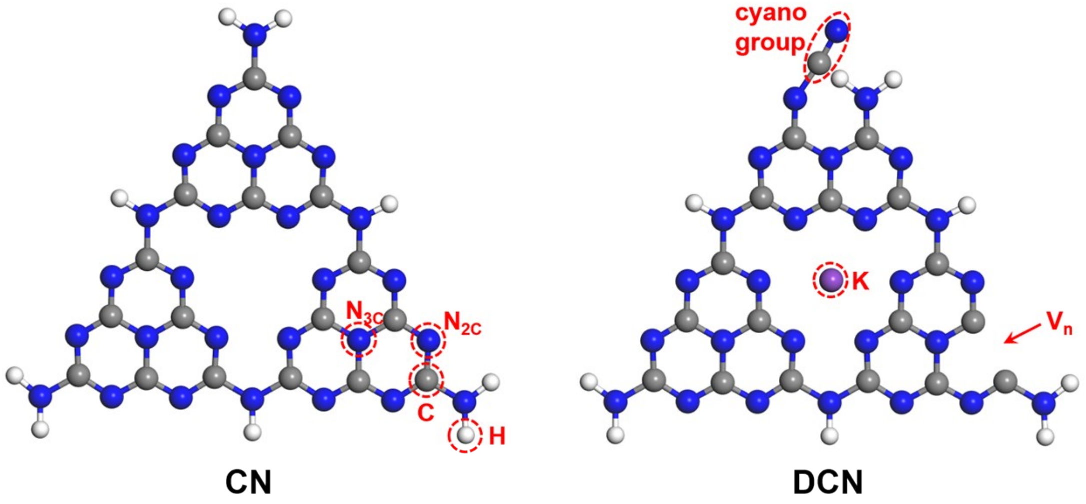

Scheme S1. Schematic atomic model of CN and DCN.

The C 1s XPS spectra (Figure S2) for CN show three fitting peaks assignable to N–C=N (288.4 eV), C–NH_x on the edges of tri-s-triazine units (x=1 or 2, 286.4 eV), and adventitious hydrocarbons (284.8 eV).[1] The intensified C–NH_x peak of DCN can be taken as an additional evidence for the formation of cyano groups since cyano groups possess similar C1s binding energies to C–NH_x.[1]

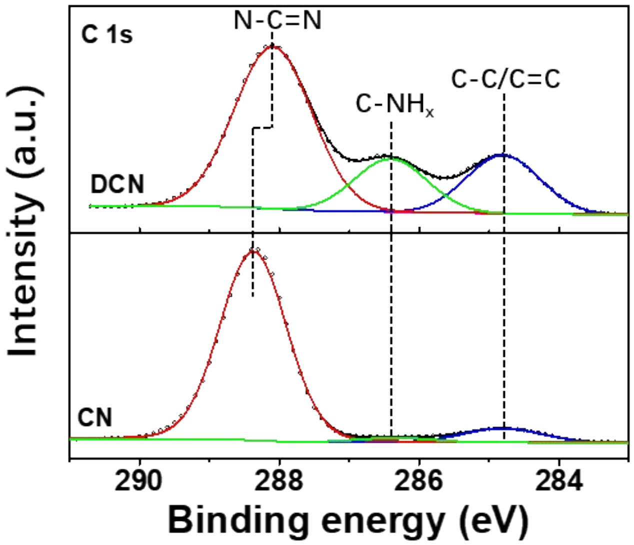

Figure S2. C 1s XPS spectra of CN and DCN.

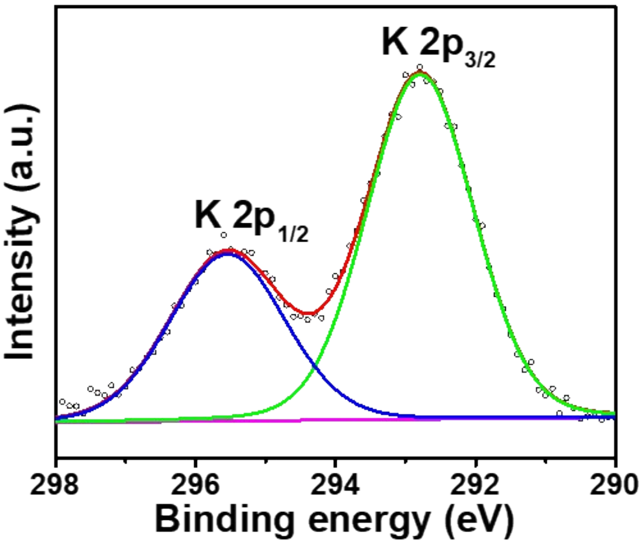

Figure S3. K 2p XPS spectrum of DCN.

According to Figure S10, the bandgap calculation is based on the fact that the transition from VB to CB for CN is direct, while the transition from V_n states (band tail states) to CB for DCN is indirect. However, it is difficult to directly figure out whether the transition from the intrinsic VB of DCN to the CB is direct or indirect because VBM at Z point is only a little bit higher than VB at G point for CN-V_n. It should be considered as a “slightly” indirect transition. Therefore, both bandgaps due to direct and indirect transitions are considered.

If the transition from the intrinsic VB of DCN to the CB is direct, the gap is calculated to be 2.70 eV (Figure 2b). In this case, the intrinsic VBM of DCN is 0.19 eV lower than the VB of CN (Figure 2d). However, if the transition is indirect, the gap is calculated to be 2.39 eV (Figure S4). Then the intrinsic VBM of DCN is 0.12 eV higher than the VB of CN. However, according to the Figure 2c, the VBM of DCN is lower than that of CN. Therefore, the transition from the intrinsic VB of DCN to the CB should be still considered as a direct one.

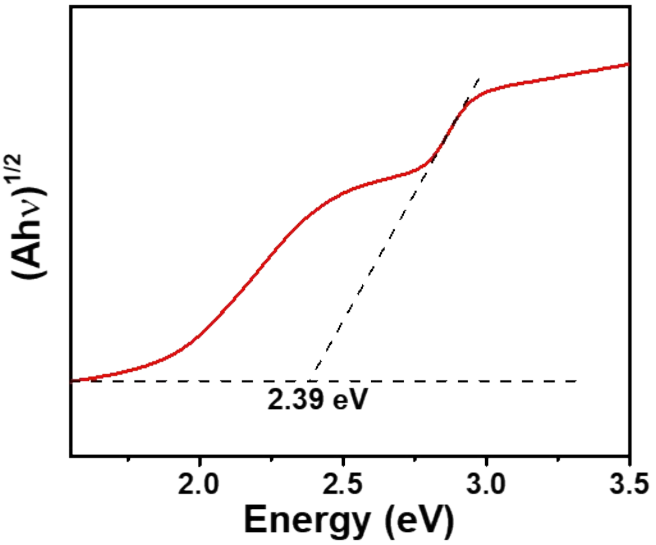

Figure S4. Tauc plot for the band gap calculation for DCN.

The VBM potential of TiO_2 (anatase) versus normal hydrogen electrode (NHE, PH = 7) is calculated by using the formula $E_{VBM\ vs.\ NHE}/V = \Phi + E_{VBM\ vs.\ Fermi} - 4.44$ ($E_{VBM\ vs.\ NHE}$ of 2.74: VBM potential of TiO_2 vs. NHE;[4] Φ of 4.5: work function of TiO_2;[5] $E_{VBM\ vs.\ Fermi}$: the difference between the VBM of TiO_2 and Fermi level).[6] Therefore, $E_{VBM\ vs.\ Fermi}$ is calculated to be 2.68 eV. However, the tested $E_{VBM\ vs.\ Fermi} = 2.85$ eV (Figure S5), which means there is an error of 0.17 eV in our VB XPS test. Then, we use this error to calibrate the VB XPS of CN and DCN in this work, as shown in Figure 2c.

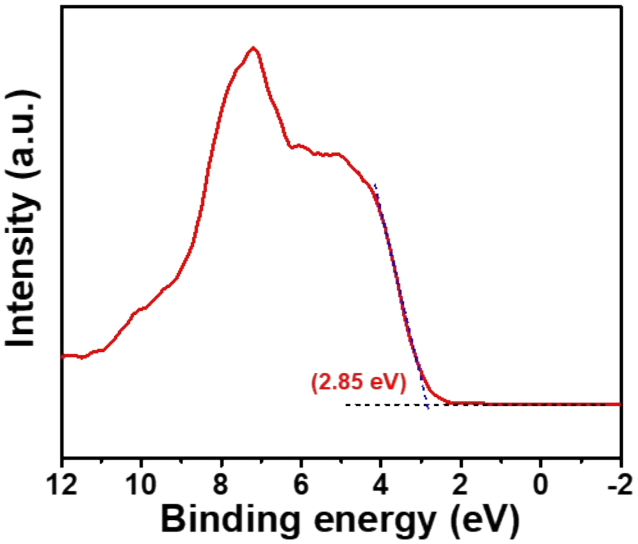

Figure S5. VB XPS spectrum of TiO_2 (anatase).

Although the as-synthesized CN samples are constructed from tri-s-triazine units, we employed another widely used CN model which is based on s-triazine because the unit cell of tri-s-triazine could contain large number of atoms, making the simulation computationally expensive.[7-11] One V_n was introduced by removing one two-coordinated N atom directly, while one cyano group was introduced by breaking one s-triazine unit according to the previous reports.[12,13] The calculated density of states (DOS) agree well with our experimental observations and the band structure of CN (Figure S10) is similar to the previous reports,[9,14] indicating a reliable simulation in this work.

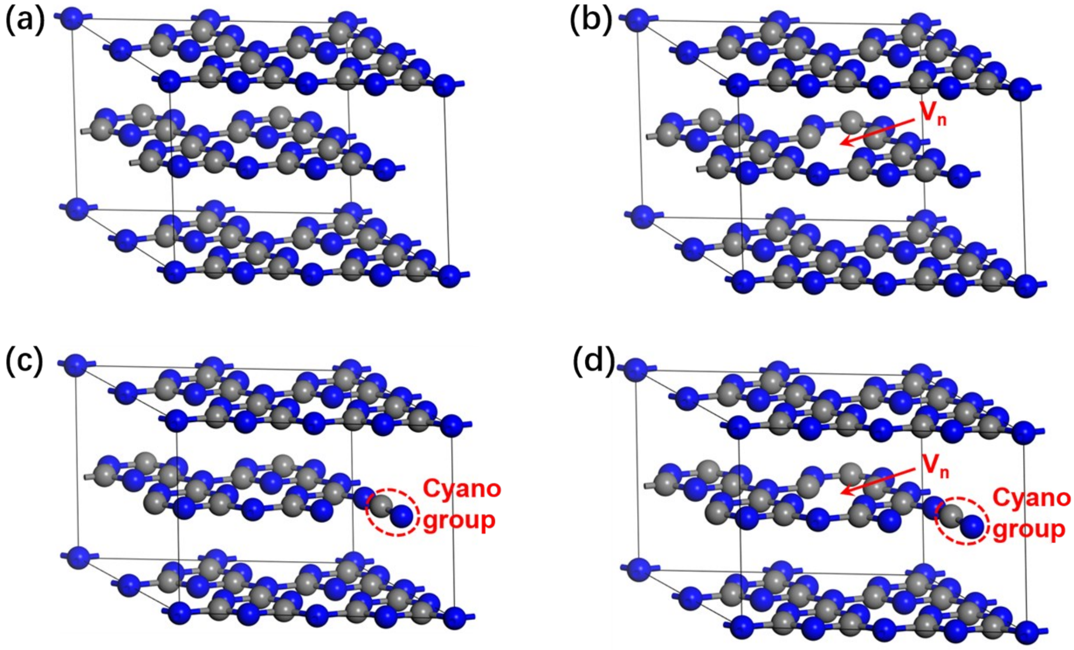

Figure S6. Computation models of CN (a), CN with one N vacancy (CN-V_n, b), CN with one cyano group (CN-cyano, c), and CN with one V_n and one cyano group (d). Gray balls, C atoms; blue balls, N atoms.

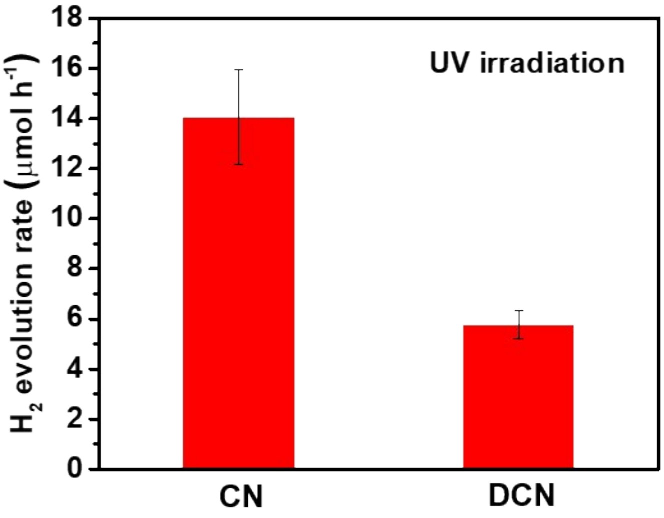

Figure S7. Photocatalytic H_2 evolution using CN and DCN under UV irradiation.

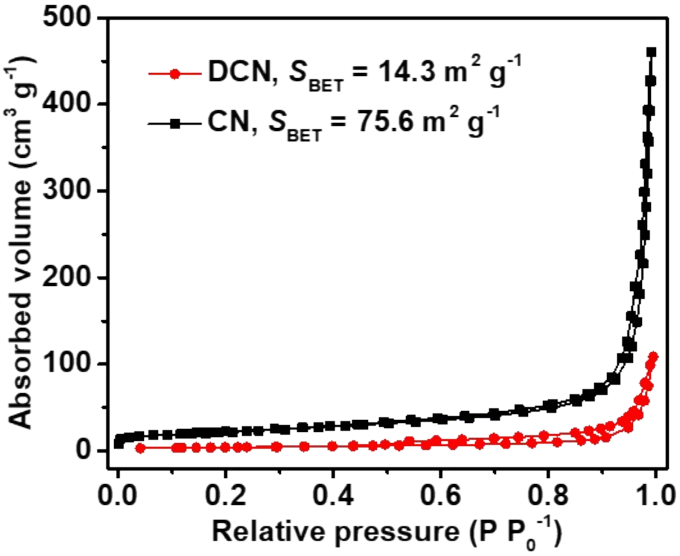

Figure S8. Nitrogen adsorption-desorption isotherms of CN and DCN.

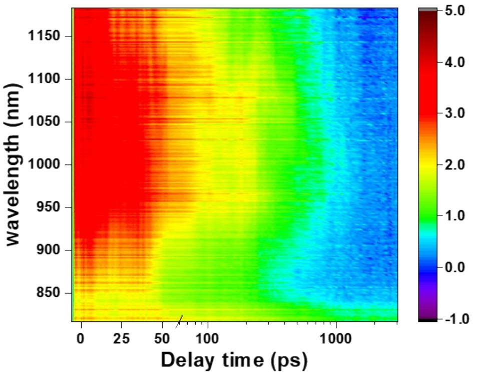

CN with 420 nm pump

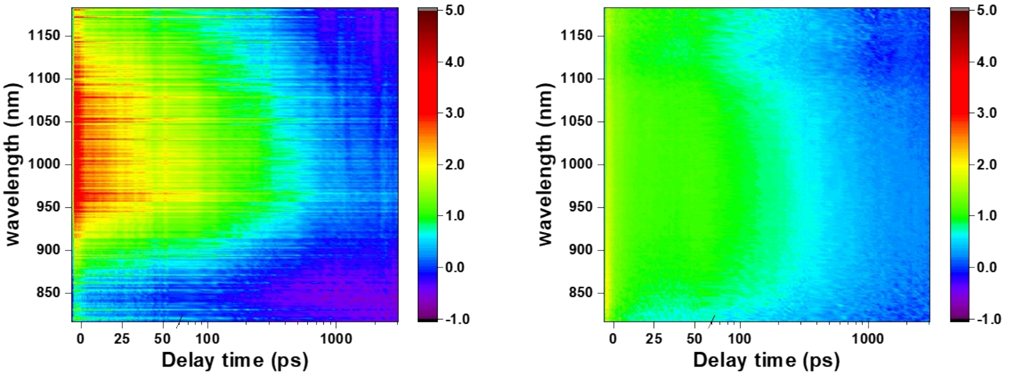

DCN with 420 nm pump

DCN with 560 nm pump

Figure S9. TA spectral mappings observed during laser flash photolyses of CN and DCN.

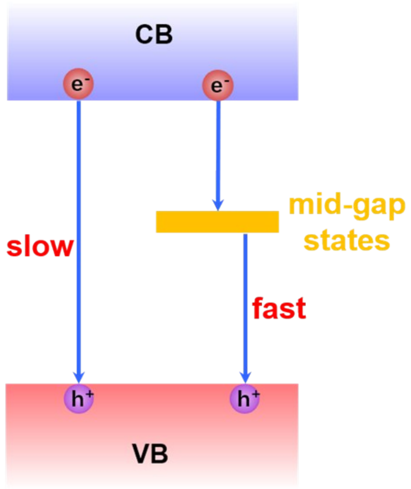

Scheme S2. Schematic diagram of Shockley-Read-Hall (SRH) recombination mediated by mid-gap states.

As shown in Figure S10, after the introduction of the cyano group, the band structures around CBM and VBM become less dispersive, reflecting the heavier photogenerated electrons and holes. This trend is in accordance with the report by Zhang et al.[13] Another interesting finding is that the introduction of the V_n results in the change of CN from a direct semiconductor to an indirect one, which may increase the electron-hole lifetime.[15]

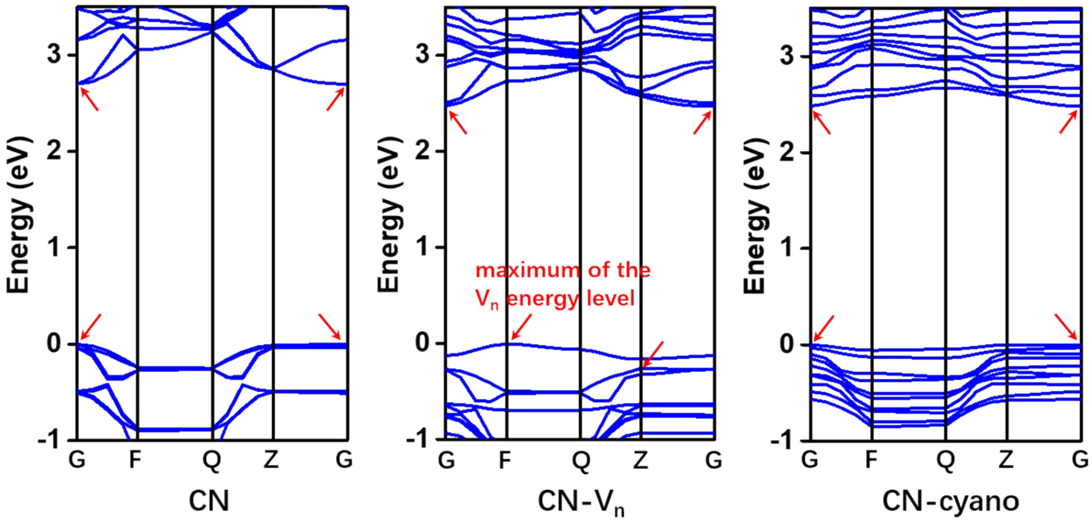

Figure S10. Calculated band structures of CN, CN-V_n, and CN-cyano. The Fermi level is taken to be zero. The red arrows mark the CBM, VBM, and the maximum of the V_n energy level.

Table S2. The effective mass of electrons and holes for CN, DN-V_n, and CN-cyano obtained from parabolic fitting to the CBM, VBM, and the maximum of the V_n energy level (marked by the red arrows in Figure S10) along a specific direction in the reciprocal space.

Species		m_e^*/m_0		m_h^*/m_0	
CN	Direction	G → F	G → Z	G → F	G → Z
	Calculation	0.26	0.67	0.41	78
	Average	0.47		39	
CN-V_n	Direction	G → F	G → Z	F → G	F → Q
	Calculation	0.42	0.95	0.91	3.5
	Average	0.69		2.2	
	Direction	–	–	Z → Q	Z → G
	Calculation	–	–	0.73	27
	Average	–		14	
CN-cyano	Direction	G → F	G → Z	G → F	G → Z
	Calculation	0.73	1.3	3.3	394
	Average	1.0		199	

As shown in Table S2, the lighter electrons (0.26 m_0) and holes (0.41 m_0) along G → F direction (in-plane) than those electrons (0.67 m_0) and holes (78 m_0) along G → Z (vertical) direction in CN indicates the fast mobility of charges within the in-plane of CN and the slow mobility of charges along the vertical direction, due to the in-plane electron delocalization of π-π conjugation and the weak electronic coupling between the spatially separated 2D layers.[14]

References:

(1) H. Yu, R. Shi, Y. Zhao, T. Bian, Y. Zhao, C. Zhou, G. I. N. Waterhouse, L. Z. Wu, C. H. Tung and T. Zhang, *Adv. Mater.*, 2017, **29**, 1605148.

(2) W. Tu, Y. Xu, J. Wang, B. Zhang, T. Zhou, S. Yin, S. Wu, C. Li, Y. Huang, Y. Zhou, Z. Zou, J. Robertson, M. Kraft and R. Xu, *ACS Sustainable Chem. Eng.*, 2017, **5**, 7260-7268.

(3) Z. Huang, F. W. Yan and G. Q. Yuan, *ACS Sustainable Chem. Eng.*, 2018, **6**, 3187-3195.

(4) W. Ong, L. Tan, Y. H. Ng, S. Yong and S. Chai, *Chem. Rev.*, 2016, **116**, 7159-7329.

(5) H. Yaghoubi, Z. Li, Y. Chen, H. T. Ngo, V. R. Bhethanabotla, B. Joseph, S. Ma, R. Schlaf and A. Takshi, *ACS Catal.*, 2015, **5**, 327-335.

(6) J. Cao, W. Nie, L. Huang, Y. Ding, K. Lv and H. Tang, *Appl. Catal. B*, 2019, **241**, 18-27.

(7) Q. Tay, P. Kanhere, C. F. Ng, S. Chen, S. Chakraborty, A. C. H. Huan, T. C. Sum, R. Ahuja and Z. Chen, *Chem. Mater.*, 2015, **27**, 4930-4933.

(8) X. Zhang, X. Xie, H. Wang, J. Zhang, B. Pan and Y. Xie, *J. Am. Chem. Soc.*, 2013, **135**, 18-21.

(9) W. Yu, D. Xu and T. Peng, *J. Mater. Chem. A*, 2015, **3**, 19936-19947.

(10) J. Liu, B. Cheng and J. Yu, *Phys. Chem. Chem. Phys.*, 2016, **18**, 31175-31183.

(11) P. Li, F. Wang, S. Wei, X. Li and Y. Zhou, *Phys. Chem. Chem. Phys.*, 2017, **19**, 4405-4410.

(12) F. Yang, D. Liu, Y. Li, L. Cheng and J. Ye, *Appl. Catal. B*, 2019, **240**, 64-71.

(13) D. Zhang, X. Han, T. Dong, X. Guo, C. Song and Z. Zhao, *J. Catal.*, 2018, **366**, 237-244.

(14) W. Yu, J. Chen, T. Shang, L. Chen, L. Gu and T. Peng, *Appl. Catal. B*, 2017, **219**, 693-704.

(15) J. Zhang, P. Zhou, J. Liu and J. Yu, *Phys. Chem. Chem. Phys.*, 2014, **16**, 20382-20386.